Supplementary Information

A Structure from Motion photogrammetry-based method to generate sub-millimetre resolution Digital Elevation Models for investigating rock breakdown features

Ankit K. Verma[1] and Mary C. Bourke[1]

[1]Department of Geography, Trinity College Dublin, The University of Dublin, Dublin, Ireland

Correspondence to: Ankit K. Verma (vermaan@tcd.ie)

S1. Guideline for DEM generation workflow in Photoscan

Stage 1: All images are loaded and reviewed in Photoscan. Data with image quality value higher than 0.5 were selected (Agisoft, 2016). The coded GCPs were detected automatically before starting batch processing of images. Local coordinates for each GCP target was entered into Photoscan. The measurement accuracy was adjusted to 0.01 mm for marker accuracy and scale bar accuracy in reference settings for experiments. This value was 0.5 mm for control target in the field. Unwanted scenes in the background or foreground of images (e.g. sky and plants) can lead to incorrect point matching. Photoscan offers a solution to mask out unwanted areas. While this can be a time-consuming process, it can be minimised with careful image acquisition.

Stage 2: Images alignment and optimisation: The program matches the common point in images and determines the camera position for each photo. A 3D sparse point cloud is generated using a least square solution (Thoeni et al., 2014; Agisoft, 2016). The error between measured GCP coordinates and estimated GCP coordinates is determined through the least squares solution (Thoeni et al., 2014). Photos were aligned with the highest alignment accuracy, generic pair pre-selection and the default per-image key and tie point limits. To generate the most accurate 3D model, it is crucial to overcome systematic dishing and doming distortions in the SfM model by correcting lens distortions (Carbonneau and Dietrich, 2016). SfM workflow performs a self-calibration using Exchangeable Image File Format (EXIF) metadata from digital images. Each image is treated as unique during the self-calibration process. The GCP errors were minimised using the camera calibration parameters to refine any distortion in the model during optimisation. PhotoScan adjusts estimated point coordinates and camera parameters, during optimisation, thus reducing the sum of reprojection error and reference coordinate misalignment error (Agisoft, 2016). Although a 3D sparse point cloud is not required for DEM generation, it is required for dense point cloud reconstruction.

Stage 3: Dense Point cloud generation: The dense point cloud is built, using estimated camera positions from sparse point cloud generated during image alignment process. A range of quality options are available, and we selected "High". This decision was based on the time required to achieve the required quality for our work. Choosing "Ultra high" can result in higher point density but increases processing time. We used "Mild" depth filtering as we wanted to reconstruct smaller breakdown features (Agisoft, 2016). The dense point cloud was used to generate the DEM.

Stage 4: Mesh and texture: Photoscan reconstructed a 3D polynomial mesh based on dense point cloud representing the rock surface. After mesh, the texture was generated. Mesh is not required for exporting DEM, but a textured mesh model is needed to generate a high-resolution orthophoto.

Table S1. Horizontal checkpoint errors in DEMs produced in error evaluation experiment.

Scale bar no.	Coded scale bar	24 mm extended area (mm)	24 mm profile corrected (mm)	24 mm without profile corrected (mm)	35 mm AdobeRGB (mm)	35 mm corner marker (mm)	35 mm jpg (mm)	35 mm masked (mm)	35 mm profile corrected (mm)	35 mm ProPhotoRGB (mm)	35 mm sRGB (mm)
S1	target 4_target 5	-0.78	-0.77	-0.73	-0.82	-0.64	0.48	-0.84	-0.82	-0.83	-0.82
S2	target 6_target 7	0.77	0.8	0.83	0.91	1.09	1.8	0.9	0.91	0.9	0.94
S3	target 8_target 9	-0.98	-0.95	-0.9	-0.91	-0.74	0.18	-0.93	-0.91	-0.93	-0.91
S4	target 10_target 11	0.35	0.42	0.44	0.45	0.61	1.72	0.43	0.45	0.43	0.47
S5	target 12_target 13	0.46	0.49	0.51	0.5	0.63	1.44	0.48	0.49	0.49	0.51
S6	target 14_target 15	-0.62	-0.65	-0.62	-0.69	-0.55	0.25	-0.7	-0.68	-0.69	-0.69
S7	target 16_target 17	0.66	0.66	0.7	0.73	0.86	1.46	0.72	0.73	0.72	0.75
S8	target 18_target 19	-0.75	-0.75	-0.71	-0.72	-0.59	-0.05	-0.73	-0.72	-0.73	-0.71
S9	target 20_target 21	0.36	0.34	0.38	0.42	0.52	1.06	0.42	0.42	0.42	0.43
S10	target 22_target 23	-0.5	-0.53	-0.5	-0.53	-0.44	0.09	-0.54	-0.53	-0.54	-0.53
S11	target 24_target 25	0.44	0.43	0.46	0.5	0.59	0.92	0.49	0.51	0.49	0.51
S12	target 26_target 27	-0.47	-0.49	-0.46	-0.48	-0.4	-0.23	-0.49	-0.48	-0.49	-0.48
S13	target 28_target 29	0.25	0.25	0.24	0.28	0.32	0.58	0.27	0.26	0.27	0.29
S14	target 30_target 31	-0.19	-0.2	-0.19	-0.23	-0.19	0.08	-0.24	-0.22	-0.24	-0.23
S15	target 32_target 33	0.24	0.25	0.25	0.28	0.32	0.5	0.27	0.28	-0.24	0.28
S16	target 34_target 35	-0.2	-0.21	-0.19	-0.24	-0.2	0.09	-0.25	-0.24	-0.24	-0.24
S17	target 43_target 44	-0.33									
S18	target 45_target 46	-0.33									
S19	target 47_target 48	-0.27									
S20	Target 49_target 50	-0.27									

Table S2. Vertical checkpoint errors in DEMs produced in error evaluation experiment.

	24 mm extended area (mm)	24 mm profile corrected (mm)	24 mm profile without corrected (mm)	35 mm AdobeRGB (mm)	35 mm corner marker (mm)	35 mm jpg (mm)	35 mm masked (mm)	35 mm profile corrected (mm)	35 mm ProPhotoRGB (mm)	35 mm sRGB (mm)
Wooden Block										
A	0.04	0.14	0.23	-0.19	-0.1	0.16	-0.05	-0.39	-0.3	-0.34
B	0.1	0.37	0.31	-0.09	0.26	-0.16	0.19	-0.19	-0.33	-0.55
C	0.28	0.28	0.33	-0.02	-0.2	-0.006	0.01	-0.05	-0.2	-0.31
D	0.09	0.26	0.36	-0.14	0.13	-0.33	0.06	-0.12	-0.16	-0.18
E	-0.24	-0.37	0.01	-0.42	-0.2	-0.56	-0.13	-0.79	-0.68	-0.67
F	-0.34	-0.1	-0.09	-0.48	-0.19	-0.12	-0.2	-0.35	-0.45	-0.67
G	-0.07	-0.009	0.01	-0.32	-0.1	-0.11	-0.13	-0.19	-0.31	-0.27
H	-0.14	-0.01	0.006	-0.41	-0.17	-0.29	-0.22	-0.56	-0.54	-0.61
I	-0.39	-0.43	-0.23	-0.37	-0.46	-0.44	-0.46	-0.79	-0.84	-0.48
J	-0.64	0.03	-0.22	-0.17	0.15	-0.2	0.05	-0.35	-0.39	-0.33
K	0.23	0.54	0.55	0.03	0.33	0.16	0.4	-0.09	0.04	0.004
L	0.39	0.68	0.47	0.25	0.47	0.28	0.45	0.16	0.2	0.39
M	0.29	0.36	0.35	0.35	0.49	0.49	0.52	0.14	0.25	0.29
N	-0.27	-0.03	-0.12	-0.17	-0.09	-0.48	-0.06	-0.14	-0.24	-0.06
O	-0.02	0.09	0.16	-0.07	0.14	-0.06	0.16	-0.11	-0.02	-0.09
P	0.9	0.8	0.9	0.59	0.35	0.68	0.43	0.54	0.63	0.58

S2. Role of image variables in DEM error

S2.1. Type of lens (prime vs zoom)

The DEMs generated from images acquired with prime lens and zoom lens were compared to explore the effect of the type of lens on DEM accuracy. For this purpose, 24 mm without profile corrected and 35 mm masked DEMs were used (Table 4). Horizontal errors were similar in DEMs generated from images taken with both lenses (Figure S1a). Horizontal RMSE for zoom lens DEM was 0.55 mm, and for prime lens, DEM was 0.59 mm. However, Vertical RMSE for the prime lens DEM (0.28 mm) was a little lower than zoom lens DEM (0.35 mm). We determined the intra-class correlation (ICC) for all the horizontal and vertical checkpoint errors (Figure S1 a and b). For horizontal checkpoint errors, ICC is 0.998. For vertical errors, it is 0.847. Reprojection error and projection accuracy were slightly lower for prime lens DEM (Table 4 and Figure S2 b and d). Dense point cloud density for the prime lens was about two times higher than for a zoom lens.

We find therefore that the use of the prime lens will yield lower errors compared to a zoom lens for SfM photogrammetry, as suggested by Mosbrucker et al. (2017). Although, this experiment suggests that there is no statisticsal significant difference in the accuracy of DEMs generated from prime and zoom lens. The slightly higher errors due to using zoom lens is acceptable considering that it offers flexibility to choose a focal length (choice depends on the field of view) and its low cost.
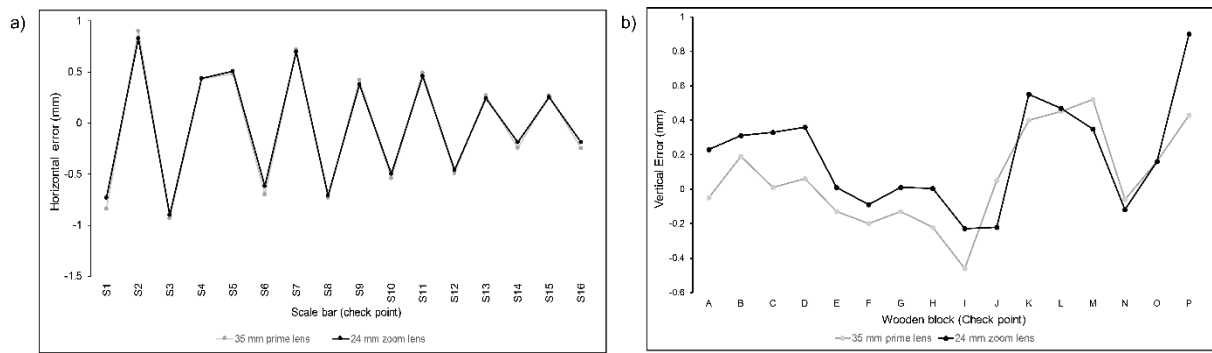
Figure S1. Comparison of horizontal and vertical checkpoint errors in DEM due to the type of lens. (a) Horizontal checkpoint error. (b) Vertical checkpoint error.
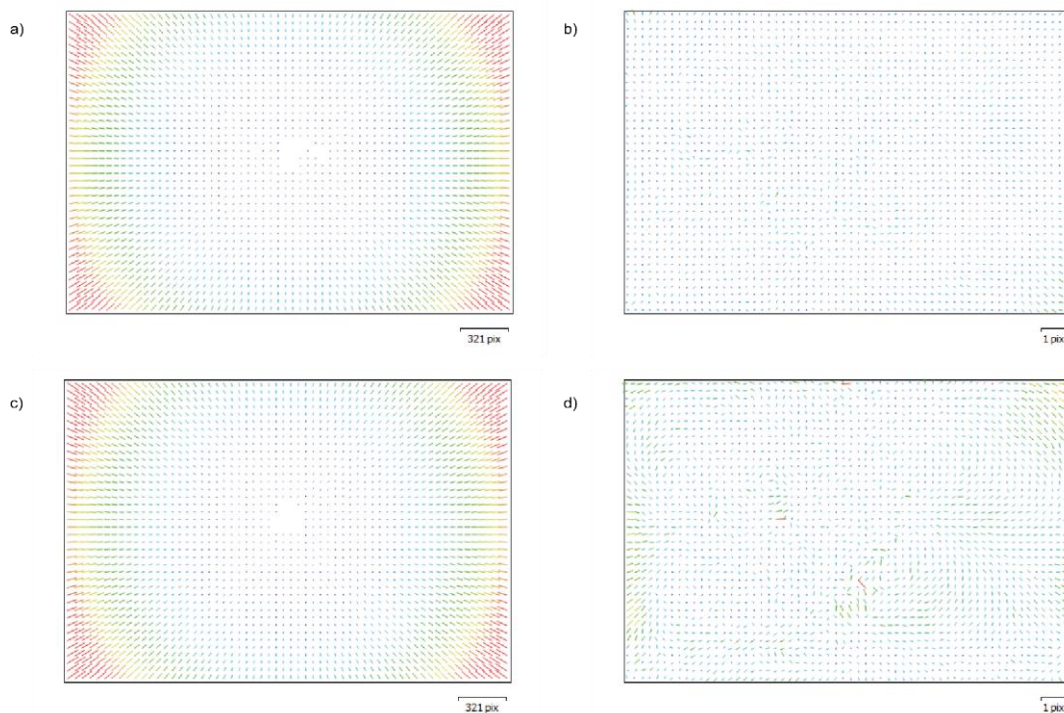
Figure S2. (a) Distortion plot for 35 mm prime lens (b) Residual error plot for 35 mm prime lens. (c) Distortion plot for zoom lens set at 24 mm. (d) Residual error plot for zoom lens set at 24 mm. In image b) and d) residual vectors are magnified by x331.

S2.2. Prior lens profile correction

The effect of prior lens profile correction in Adobe Lightroom on the accuracy of DEM was explored. We used 35 mm profile corrected, 35 mm ProPhotoRGB, 24 mm profile corrected and 24 mm without profile corrected DEMs for comparison (Table 4). Images acquired from 35 mm lens and 24 mm lens were corrected for lens distortion in Lightroom. The horizontal and vertical checkpoint was very similar for a zoom lens (Figure S3 c and d). ICC for horizontal (0.999) and vertical errors (0.947) were very high. For a prime lens, lens profile correction

did not affect horizontal and vertical checkpoint error (Figure S3 a and b). ICC for horizontal (0.988) and vertical errors (0.981) were very high for fixed focus lens as well. All the others DEM parameters presented in Table 4 were not affected due to lens profile correction. We find that there was no significant difference observed in DEM accuracy due to prior lens profile correction in images.
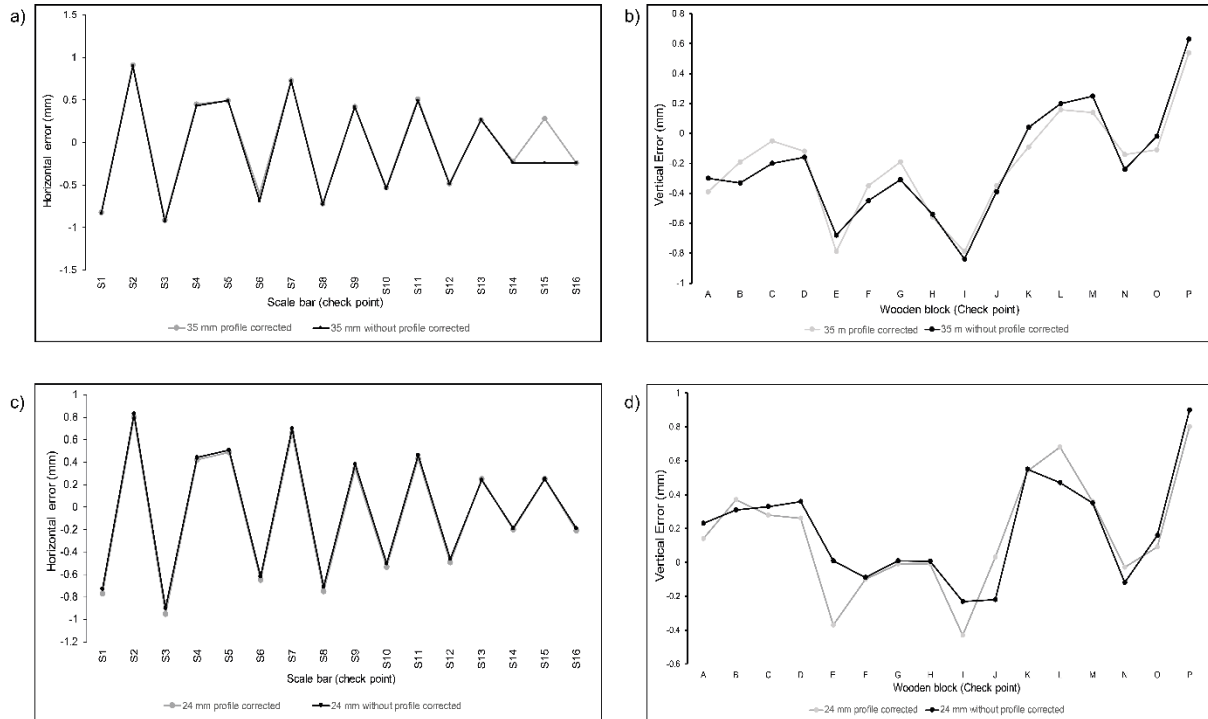
Figure S3. Comparison of horizontal and vertical checkpoint errors in DEM due to lens profile correction. (a) and (b) Horizontal and vertical checkpoint errors for a zoom lens. (c) and (d) Horizontal and vertical checkpoint errors for a prime lens.

S2.3. Colour space of images

In this experiment, the effect of colour space (Katoh, 2005;Korytkowski and Olejnik-Krugly, 2017) on DEM accuracy was investigated. Images acquired from 35 mm prime lens in sRGB, AdobeRGB, and proPhotoRGB was used to make DEMs. We compared 35 mm ProPhotoRGB, 35 mm sRGB, 35 mm AdobeRGB DEMs (Table 4). Horizontal checkpoint errors were very similar for all the DEMs (Figure S4 a). However, vertical errors for AdobeRGB DEM were slightly lower than ProPhotoRGB and sRGB DEMs (Figure S4 b). ICC for horizontal and vertical errors were 0.995 and 0.960. There was negligible difference between ProPhotoRGB and sRGB DEMs, but AdobeRGB DEM had slightly higher vertical accuracy. Mosbrucker et al. (2017) suggested that AdobeRGB images take less time to match points. In this experiment, all the colour spaces (images) took equal time to match points. AdobeRGB and sRGB images have 1% higher tie points than ProPhotoRGB images, but the dense point cloud density and DEM resolution was same for all colour space images. AdobeRGB images had lower reprojection errors compared to ProPhotoRGB and sRGB images. We, therefore, recommend using AdobeRGB colour space for images.
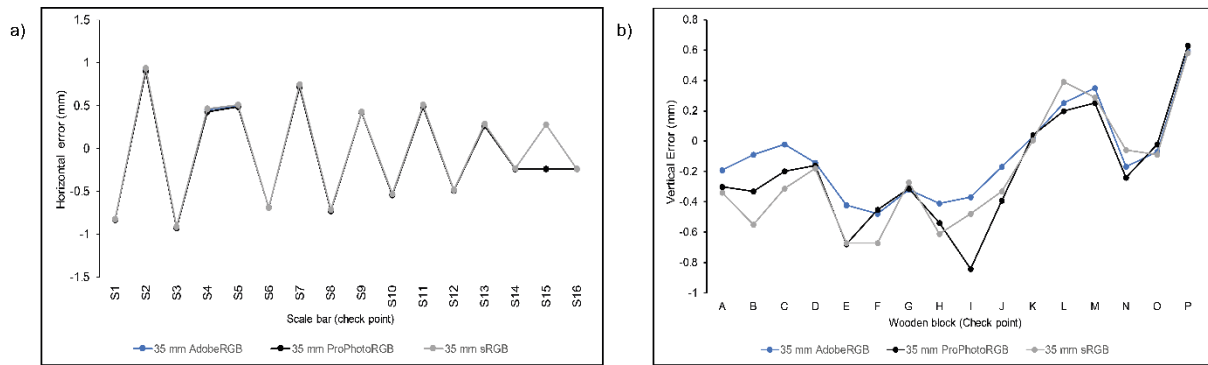
Figure S4. Comparison of horizontal and vertical checkpoint errors in DEM due to colour space. (a) Horizontal checkpoint error. (b) Vertical checkpoint error.

S2.4. Dense point cloud quality setting in Photoscan

In this experiment, the effect of dense point quality setting (or in other words point density) on DEM accuracy was assessed. We compared "high" and "medium" dense point cloud quality setting in Photoscan. We used 35 mm masked and 35 mm ProPhotoRGB DEM for comparison (Table 4). "High" quality setting produced four times higher point density and two times higher DEM resolution compared to "medium" quality setting. Horizontal errors for both quality settings were very similar (Figure S5 a). However, vertical errors for "high" quality setting were lower than "medium" quality setting (Figure S5 b). ICC for horizontal error (0.989) was very high but for vertical accuracy (0.782) was lower. It took 6.7 times longer to produce "high" quality DEM compared to "medium" quality DEM. Both the DEMs had vertical RMSE less than 0.5 mm.

If time is a constraint, then we recommend choosing "medium" dense point cloud quality setting to generate DEM as there is no significant loss of DEM accuracy.
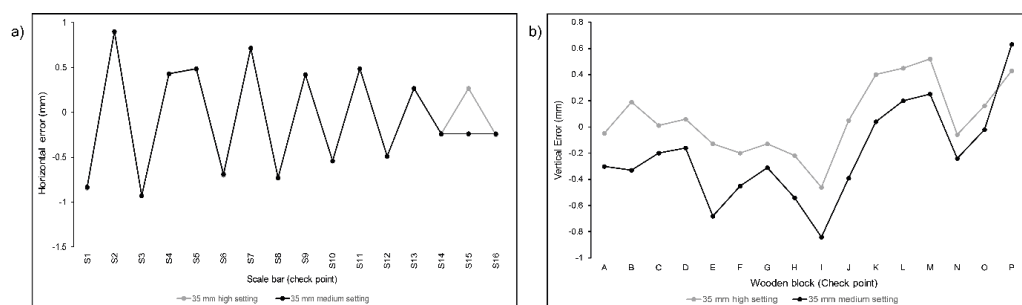
Figure S5. Comparison of horizontal and vertical checkpoint errors in DEM due to dense point cloud quality setting in Photoscan. (a) Horizontal checkpoint error. (b) Vertical checkpoint error.

S2.5. Image file format (jpg vs tiff)

The effect of image file format (compression) on the accuracy of DEM was compared in this experiment. We examined 35 mm jpg and 35 mm ProPhotoRGB DEMs (Table 4). Jpg format images produced higher horizontal errors in DEM compared to tiff format images (Figure S6 a). Vertical errors were slightly lower for jpg DEM

compared to tiff DEM (Figure S6 b). ICC for horizontal errors (0.685) was very low and vertical errors (0.890) was high. Reprojection error for jpg DEM was about six times higher, and projection error was eight times higher compared to DEM generated using uncompressed tiff images (Table 4). Jpg image format significantly increases error in DEMs. We recommend using tiff format images.
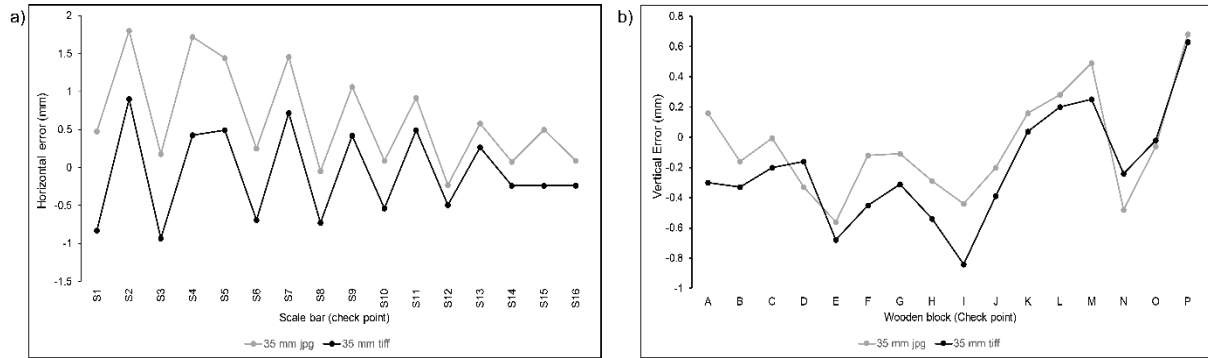
Figure S6. Comparison of horizontal and vertical checkpoint errors in DEM due to image file format (compression). (a) Horizontal check point error. (b) Vertical checkpoint error.

S2.6. The position of the control target with respect to subject

In this experiment, the effect of the position of the control target with respect to subject of interest on DEM accuracy was explored. We compared 35 mm corner target and 35 mm masked DEMs (Table 4). We find that the position of the control target had an almost negligible effect on horizontal and vertical errors (Figure S7 a and b). ICC for horizontal errors (0.988) and vertical errors (0.982) was very high.
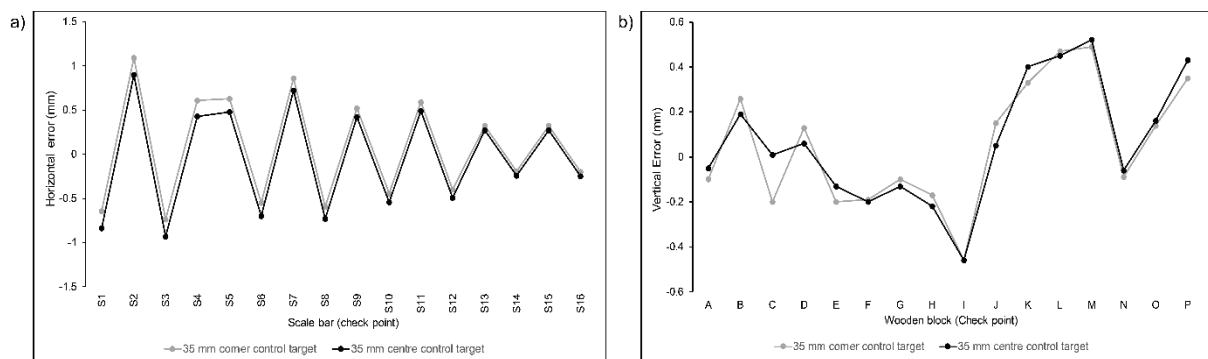
Figure S7. Comparison of horizontal and vertical checkpoint errors in DEM due to the position of the control target. (a) Horizontal checkpoint error. (b) Vertical checkpoint error.

S2.7. Masking

The role of masking of images was compared on the DEM error in this experiment. We used 35 mm corner target and 35 mm masked DEMs for this comparison (Table 4). Masking had an almost negligible effect on Horizontal and Vertical errors in DEM (Figure S7 a and b). In this experiment, masking of images did not reduce the time in the generation of DEM.

References

Photoscan, A.: Agisoft Photoscan User Manual Professional Edition, Version 1.2, Agisoft LLC, 2016.

Carbonneau, P. E., and Dietrich, J. T.: Cost-effective non-metric photogrammetry from consumer-grade sUAS: implications for direct georeferencing of structure from motion photogrammetry, Earth Surface Processes and Landforms, 2016.

Katoh, N.: Extended colour space for capturing devices, Proc. 10th Congress of the International Colour Association, AIC Colour, 2005, 647-652,

Korytkowski, P., and Olejnik-Krugly, A.: Precise capture of colors in cultural heritage digitization, Color Research & Application, 42, 333-336, 2017.

Mosbrucker, A. R., Major, J. J., Spicer, K. R., and Pitlick, J.: Camera system considerations for geomorphic applications of SfM photogrammetry, Earth Surface Processes and Landforms, 2017.

Thoeni, K., Giacomini, A., Murtagh, R., and Kniest, E.: A comparison of multi-view 3D reconstruction of a rock wall using several cameras and a laser scanner, The International Archives of Photogrammetry, Remote Sensing and Spatial Information Sciences, 40, 573, 2014.